International Journal of Climatology

International Journal of Climatology RMetS

RESEARCH ARTICLE

Projected Changes in Diurnal Temperature Range Over India Using a Coupled Ocean–Atmosphere Regional Climate Model

C. B. Jayasankar[1,2] | Vasubandhu Misra[1,2,3]

[1]Center for Ocean-Atmospheric Prediction Studies, Florida State University, Tallahassee, Florida, USA | [2]Florida Climate Institute, Florida State University, Tallahassee, Florida, USA | [3]Department of Earth, Ocean and Atmospheric Science, Florida State University, Tallahassee, Florida, USA

Correspondence: C. B. Jayasankar (cbjayasankar@gmail.com)

Received: 12 October 2023 | **Revised:** 7 November 2024 | **Accepted:** 11 November 2024

Funding: This work was supported by NASA Earth Science Division grant numbers: 80NSSC19K1199, 80NSSC22K0595.

Keywords: climate change projections | diurnal temperature range | dynamical downscaling | India | regional climate model

ABSTRACT

This study investigates the projected changes in the diurnal temperature range (DTR) over India and explains its considerable spatial heterogeneity from a 20-km resolution coupled regional climate model (RSM-ROMS) integration. The RSM-ROMS is driven at the lateral boundaries by the Community Climate System Model version 4 (CCSM4) model. Observations reveal spatial heterogeneity in DTR trends with significant declining trends at many grid points interspersed with areas of either increasing or insignificant trends of DTR during each of the four seasons. The present-day simulations from RSM-ROMS show reasonable skill in simulating the daily maximum temperature (Tmax) and minimum temperature (Tmin) over India. Our results show a significant decrease in DTR over the Gangetic Plains in boreal winter and fall seasons and over southeastern India during boreal summer in the projected mid-21st century climate under the RCP 8.5 emission scenario. The future reduction in DTR over Region-1 (over Bihar and the eastern regions of Uttar Pradesh) during December–February (−0.86°C) and over Region-3 (over the rain shadow regions of Peninsular India) during June–September (−0.49°C) is attributed to large changes in surface radiative fluxes, with some of the decrease in downward short wave flux attributed to an increase in high cloud cover at the time of Tmax while there is a considerable increase in downward longwave flux in the mid-21st century climate. The enthalpy fluxes at the time of Tmax also act to reduce the rate of its warming. As a result, the warming rate of Tmax is less compared with the corresponding warming rate of Tmin, which leads to a reduction of the DTR in some regions that display a significant reduction in future climate. In contrast, Region-2 (over Rajasthan) and Region-4 (over northeast India) exhibit insignificant DTR changes in the mid-21st century climate for lack of asymmetrical changes in Tmin and Tmax.

1 | Introduction

The increase in global mean temperatures with the corresponding increase in greenhouse gas (GHG) emissions is a major concern across the globe. Many studies have noted that the changes in the daily maximum (Tmax) and minimum surface temperatures (Tmin) are equally important metrics to monitor and project climate change (Dai, Trenberth, and Karl 1999; Braganza, Karoly, and Arblaster 2004). The trends in daily mean temperature can be caused by trends in either maximum or minimum temperatures or by a combination of the trends in both. The difference between daily maximum and minimum temperatures denoted as the diurnal temperature range (DTR), and the variations in the DTR can have a significant impact on various sectors like agriculture, human health, water resources, and so forth (Wilkens and

Singh 2001; Lobell, Bonfils, and Duffy 2007; Yang et al. 2013; Hamal et al. 2021). For example, grain filling rates of wheat are more responsive to Tmin than Tmax, with higher DTR likely to boost yields (Wilkens and Singh 2001; Lobell and Ortiz-Monasterio 2007). However, increased DTR has a clear detrimental effect on yields in various major rice and maize-growing regions such as India and the United States, respectively (Lobell, Bonfils, and Duffy 2007).

Previous studies show that DTR is declining across various parts of the globe and this decline is attributed to the fact that the Tmin has increased at a faster rate compared with Tmax (Karl et al. 1993; Easterling et al. 1997; Vose, Easterling, and Gleason 2005; Doan et al. 2022). This faster increase in Tmin (night-time temperature) is attributed to the increases in cloudiness, precipitation and soil moisture (Karl et al. 1993; Easterling et al. 1997; Dai, Trenberth, and Karl 1999). Over India, many of the earlier studies show that the DTR is increasing (Rupa Kumar, Krishna Kumar, and Pant 1994; Roy and Balling 2005; Bhutiyani, Kale, and Pawar 2007; Rai, Joshi, and Pandey 2012; Vinnarasi et al. 2017; Jaswal, Kore, and Singh 2016) and a few other studies suggest a decrease in DTR over certain areas over India (Jhajharia and Singh 2011; Prakash and Norouzi (2020); Mall et al. 2021). For example, Rai, Joshi, and Pandey (2012) conducted a study utilising datasets from 122 stations across India, and their findings revealed that the DTR shows an increasing trend across all seasons. They also found the largest increasing trends in DTR during the winter, whereas the smallest increasing trends occurred during the post-monsoon period. Similarly, Rupa Kumar, Krishna Kumar, and Pant (1994) found an increasing trend in DTR across 121 stations in India with the rate of rise being faster for Tmax than Tmin. Roy (2019) showed that across most of India, DTR exhibits positive trends during the drier months in the first half of the year but shifts to negative trends in the later half of the year. Shahfahad et al. (2023) found that there is a decline in the DTR trend in megacities such as Delhi and Mumbai, which is accompanied by an increased trend in the frequency of extreme temperature events, potentially increasing vulnerability to heat waves. However, Jhajharia and Singh (2011) suggested that a reduction in sunshine duration may cause a decrease in DTR over Northeastern areas of India. Mall et al. (2021) found a decline in DTR over areas of the Gangetic Plain between 1991 and 2016, which they attributed to a decrease in solar radiation. Joy and Satheesan (2022) investigated the influence of soil moisture on DTR and discovered that there is significant negative feedback on DTR in central and northern India. Hamal et al. (2021) demonstrated a decreasing trend in the observed annual DTR across the southern slope of the Central Himalayas. However, their findings also revealed that the CMIP6 models project a more rapid decline in DTR under the SSP5-8.5 scenario compared with the SSP2-4.5 and SSP1-2.6 scenarios. On the other hand, multi-model ensemble mean (MME) from 36 state-of-the-art CMIP6 models exhibit a decreasing trend in DTR (from −0.06°C/decade to −0.18°C/decade) during 1980–2014 over India (Huang et al. 2023, in their Figure S5) after it was confirmed that overall CMIP6 models verified with observations that global DTR trends are decreasing between 1980 and 2014. This result should be noted with the fact that CMIP6 models are coarse in spatial resolution which limits the model's ability to effectively represent the observed spatial heterogeneity in the trends of DTR across India. Furthermore, Huang et al. (2023) indicate significant inter-model variations in the spatial variability of DTR.

In a related study, Sillmann et al. (2013) showed that the annual averaged DTR in the CMIP3 and CMIP5 models were significantly underestimated across South Asia than the gridded observational indices data set (HadEX2). The Global General Circulation Models (GCMs) face difficulties in capturing the magnitude of the observed asymmetric trends in Tmin and Tmax, and hence underestimate the DTR changes (Stone and Weaver 2002; Braganza, Karoly, and Arblaster 2004). Various climate models project notable future changes in the DTR (Stone and Weaver 2003; Lobell, Bonfils, and Duffy 2007). Based on the analysis of both observations and model simulations, Solomon et al. (2007) indicate that the future DTR is likely to continue to decrease over global land areas which is linked to increases in cloudiness. In a study, Doan et al. (2022) used a convection-permitting regional climate model to explain the potential cause of DTR decline over the Kanto Plain (in Japan) and the Malaysian peninsula. They demonstrated that the higher daytime cloudiness in warmer climates reduces the insolation, resulting in the under-warming of Tmax. By using a GCM, Zhou et al. (2008) however found that a significant reduction in the DTR over the Sahel region is attributed to the decrease of soil emissivity which warms Tmin much faster than Tmax.

Lal, Srinivasan, and Cubasch (1996) utilised the ECHAM3 atmospheric model coupled with a large-scale geostrophic ocean model and obtained a notable future (i.e., mid-21st century) decrease in the DTR over India in winter. Interestingly, they did not observe significant trends in DTR during the monsoon season. Lindvall and Svensson (2015) show that the MME of CMIP5 models exhibits a significant reduction (ranging between −0.5°C and −1.0°C) in annual averaged DTR at the end of the 21st century (2070–2099) throughout India under the Representative Concentration Pathway (RCP) 8.5 scenario compared with the 1970–1999 period. Using CMIP5 model simulations, Singh, Chaturvedi, and Mall (2023) showed a heterogeneous projected change in DTR, however, there is a consistent decline over northern India and the highest decline is found during winter and pre-monsoon season. Using the MME of eight CMIP6 models, Liu et al. (2022) found a consistent future reduction in DTR throughout India across three different emission scenarios. Using PRECIS regional climate modelling system, Revadekar et al. (2012) show that the DTR area averaged over India is likely to decrease during winter and pre-monsoon months at the end of the 21st century under future warming scenarios. However, the DTR trend is highly heterogeneous in India. The large and diversified terrain of India, combined with distinct vegetation cover and soil types, and a varied evolution of the monsoon, causes substantial differences in surface temperature trends across the country. The global GCMs may not be therefore good enough to capture this heterogeneity in the projected DTR changes due to its coarse spatial resolution. Therefore, many of the earlier studies using coarser models, projected area averaged DTR changes across India and avoid the discussion of the spatial variability of DTR trends (e.g., Revadekar et al. 2012; Lindvall and Svensson 2015; Liu et al. 2022).

In this work, by using a relatively high-resolution coupled RCM (at 20 km grid spacing), we seek to investigate the anticipated

future changes in DTR over India across different seasons in the mid-21st century under RCP 8.5 scenario. For this purpose, we intend to focus on sub-regions of India where the observed trend in DTR exhibits significant trends. In addition, we also discuss the plausible factors responsible for the projected future changes.

2 | Model and Datasets

2.1 | Coupled Regional Climate Model

This study utilised a 20-km resolution coupled RCM simulations from dynamical downscaling set up over India following Jayasankar, Misra, and Karmakar (2023) hereafter referred to as RSM-ROMS. RSM-ROMS otherwise the Regional Spectral Model (RSM; Juang and Kanamitsu 1994; Misra, Mishra, and Bhardwaj 2018) coupled with the Regional Ocean Modelling System (ROMS, Shchepetkin and McWilliams 2005) is an extensively used tool for regional climate modelling studies (Li and Misra 2014). The details of RSM and ROMS are described in Table 1. There is no usage of flux correction during the RSM-ROMS integration for this study. Both the RSM and ROMS models are built upon an identical grid with a resolution of 20-km to avoid the flux coupler. This approach enables a direct interchange of atmospheric fluxes and sea surface temperature (SST) amongst the two model components at each hour of the model integration, eliminating the need for interpolation.

TABLE 1 | Outline of the physics used in RSM-ROMS.

Physical parameterisation	Reference
Atmospheric model (Regional Spectral Model)	
Shortwave radiation	Chou and Suarez (1994)
Longwave radiation	Chou and Lee (1996)
Clouds (explicit)	Zhao and Carr (1997)
Deep convection	Moorthi and Suarez (1992)
Shallow convection	Tiedtke (1983)
Boundary layer	Hong and Pan (1996)
Gravity wave drag	Alpert et al. (1988)
Land surface	Ek et al. (2003)
Ocean model (Regional Ocean Modelling System)	
30 vertical sigma levels on horizontal staggered Arakawa-C grid	Haidvogel et al. (2000) and Shchepetkin and McWilliams (2005)
Boundary layer formulation K-profile	Large, McWilliams, and Doney (1994)
Turbulence closure model	Mellor and Yamada (1982)
Generic length-scale parameterization	Umlauf and Burchard (2003)
Second order biharmonic horizontal diffusion	Ezer, Arango, and Shchepetkin (2002)

The initial and the time-varying lateral boundary conditions for both the atmosphere and the ocean are derived from the CCSM4 model that participated in the CMIP5. The CCSM4 coupled model is widely utilised for the dynamical downscaling over the Indian region because of its greater skill in simulating the climate of the region (Jayasankar, Rajendran, and Surendran 2018). We have generated two sets of 20-years simulations: (a) historical simulation (1986–2005) and (b) mid-21st century simulation (2041–2060). The future simulations are based on the highest GHG emission scenario that is, RCP 8.5 scenario. Since the focus is on terrestrial DTR, we provide some further details on the NOAH land surface model (Ek et al. 2003), which is used in the RSM-ROMS simulations of this study. The NOAH land surface scheme fundamentally uses bulk aerodynamic formulas to compute the surface enthalpy fluxes. However, these fluxes are scaled by the corresponding resistances where the resistance is due to aerodynamic resistance while resistance for evaporative flux is additionally a function of stomatal conductance and canopy resistance that includes heat stress (air temperature), dry air stress (air humidity) and dry soil stress (soil moisture). There are four soil layers (10, 30, 60 and 100 cm thick), with surface skin temperature, total soil moisture in each layer (volumetric), soil temperature in each layer, canopy water content, snowpack water equivalent content and snowpack depth being the prognostic quantities of the scheme. The soil temperature and moisture are computed using one-dimensional heat conduction and Richardson's equation, respectively. In addition to the enthalpy fluxes, the NOAH land surface scheme also provides upward longwave and shortwave radiative fluxes.

2.2 | Validation Datasets

We use the India Meteorological Department (IMD) gridded minimum and maximum temperature data (Srivastava, Rajeevan, and Kshirsagar 2009) for the period 1986–2022 for the validation of the RCM simulation. Srivastava, Rajeevan, and Kshirsagar (2009) interpolated data from 395 stations using Shepard's angular distance weighting algorithm, producing gridded data with a resolution of 1°×1° up to 2007. Subsequently, the number of stations was lowered to around 180. The model simulations were re-gridded to the resolution of IMD observation for verification. In addition, we also utilised the 0.5° ×0.5° daily maximum and minimum temperature data from the Climate Prediction Center (CPC) Global Unified Temperature dataset (from their website https://psl.noaa.gov). The CPC data utilises the same data through the Global Telecommunication System as the IMD dataset and is gridded using the Shepard Algorithm. To validate the simulated 2-m air temperature, we used monthly Climate Research Unit Timeseries (CRU TS) version 4.07 data (Harris et al. 2020). The 0.1° ×0.1° resolution Integrated Multi-Satellite Retrievals for Global Precipitation Mission version 6 (IMERG; Huffman et al. 2019) precipitation data at ~3.5-month latency (final product) is used to generate a Taylor diagram to validate the model simulated precipitation. We utilized hourly ECMWF Reanalysis v5 (ERA5; Hersbach et al. 2020) dataset to obtian Tmax an Tmax and Tmin over the ocean. Finally, we also make use of the Optimally Interpolated SST v2 (OISST) following Huang et al. (2021), which is available at 0.25° ×0.25° for verification of the SST from the model simulations.

3 | Results and Discussion

3.1 | Observed DTR Climatology and Trends

Using IMD observations, we estimated the spatial distribution of the 37-year mean climatology of the DTR over India (Figure 1a–d) across four seasons (DJF: December–January–February, MAM: March–April–May, JJAS: June–July–August–September and ON: October–November[1]). During the DJF, MAM and ON seasons, central and northwest India experiences higher DTR (>15°C) compared with other regions of the country (Figure 1a,b,d). In contrast, Peninsular India and the eastern coast exhibit comparatively lower DTR values. During the JJAS season, the western coast, northeast India and the northern parts of the east coast exhibit lower DTR values compared with other regions of the country (Figure 1c). Furthermore, we estimated the observed linear trend in DTR across India using IMD observations. Figure 1e–h depicts the spatial pattern of the observed DTR trend during the 37-year period from 1986 to 2022. The Theil-Sen trend estimator is used to estimate the trend and the Mann–Kendall test is used to estimate its significance. There is a considerable spatial heterogeneity in the observed DTR trend across India during all the seasons. But generally, the trends in DTR are consistent across seasons, with parts of northeast, central and southern India exhibiting a positive trend, whereas the rest of the country shows a negative trend with exceptions over Jammu and Kashmir, parts of Karnataka and Andhra Pradesh showing some seasonality.

We chose four different locations for this study (Figure S1) based primarily on the spatial patterns of the observed trends which are statistically significant at least one season (Figure 1): Region-1 (over Bihar and the eastern regions of Uttar Pradesh), Region-2 (over Rajasthan), Region-3 (over the rain shadow regions of Peninsular India) and Region-4 (northeast India). Region-1 is a part of the Indo-Gangetic plain, which receives plenty of rainfall during the monsoon. The average annual temperature in Region-1 is between 20.1°C and 25.0°C. Region-2 is an arid region (i.e., Thar desert) and the average annual temperature is between 25.1°C and 26.7°C. Region-3 is located in peninsular India, with the majority of the area being arid and some parts of it being tropical with an average annual temperature of above 26.7°C. The area-averaged observed trend over Region-3 is not statistically significant in any season, though some grid points are significant in DJF and JJAS. However, a significant projected change is expected by the mid-21st century. Region-4, located in northeast India, is characterised by complex topography, and most of the areas are under a hilly ecosystem. This region's annual average temperature ranges from 14.1°C to 25.0°C. In terms of the trend in DTR, Region-4 exhibits a contrasting positive trend compared with the predominantly negative trend observed in other regions.

There is a significant decreasing trend observed over Region-1 during the DJF, MAM and ON seasons, which varies from −0.1°C/decade to −0.52°C/decade across the seasons (Figure 1). In examining the corresponding trends in Tmin and Tmax (Figure S2) we find that in Region-1, the trend in Tmin is positive while it is negative for Tmax in DJF which explains the corresponding decreasing trend in DTR (Figure 1e). Similarly in other seasons of the year, the different trends in Tmin and Tmax reflect the reducing trend of DTR over Region-1. It is found that most parts of Region-2 (the region with high climatological DTR) also show a significant decreasing trend in DTR across all seasons (ranging between −0.11°C/decade to—0.41°C /decade). Notably, the ON season shows the highest decreasing trend of DTR over Region-2 (<−0.41°C/decade). This reducing trend in DTR over Region-2 becomes obvious from the fact

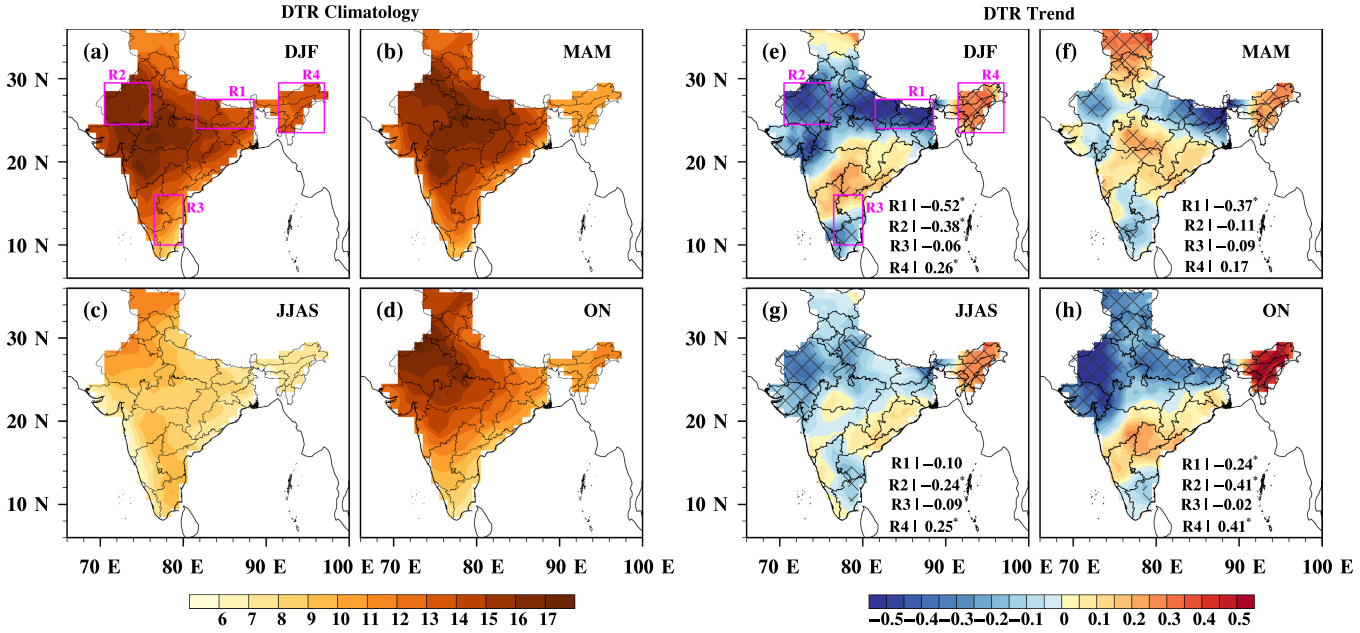

FIGURE 1 | Spatial distribution of 37-years (1986–2022) observed climatology of the diurnal temperature range (°C, a–d) and trend (°C/decade) in the DTR (e–h) for (a, e) DJF, (b, f) MAM, (c, g) JJAS and (d, h) ON seasons. The hatched areas represent trends significant at 5% significance level ($p = 0.05$) using the Mann–Kendall test. The Theil-Sen trend for area averaged DTR over four regions (Region-1—R1, Region-2—R2, Region-3—R3 and Region-4—R4) outlined in (a) and (e) are shown in each subfigure with * indicating trends are significant at 5% significance level. [Colour figure can be viewed at wileyonlinelibrary.com]

that the consistent warming trend in Tmin across all seasons (Figure S2a–d) is asymmetric to the statistically insignificant cooling trend of Tmax for most of the year with a weaker warming trend in MAM (Figure S2e–h). During the DJF and ON seasons, a majority of North and Northwest India and Southern Peninsular India display a significant decreasing trend in DTR (Figure 1). However, during the MAM season, Jammu and Kashmir, Northern Himachal Pradesh and Madhya Pradesh show a notable increasing trend in DTR. Also, during the JJAS season, there is a significant decreasing trend (−0.09°C/decade) observed over Region-3. Region-4 exhibits a significant increasing trend in DTR across all four seasons (ranging between −0.17°C/decade to −0.41°C/decade), with the ON season showing the highest increasing trend (0.41°C/decade) which is consistent with the results following Jhajharia and Singh (2011). They showed that Thakurbari station located in Assam exhibited a significant increasing trend in DTR (1973–2000) during the October–November months. These results suggest that regions with high DTR climatology, such as Region-2, are experiencing a decrease in DTR, whereas regions with slightly lower climatological DTR like Region-4, are experiencing enhanced DTR over time. These spatially heterogeneous trends in DTR across India can be understood from the corresponding differences in the trends between Tmin and Tmax shown in Figure S2.

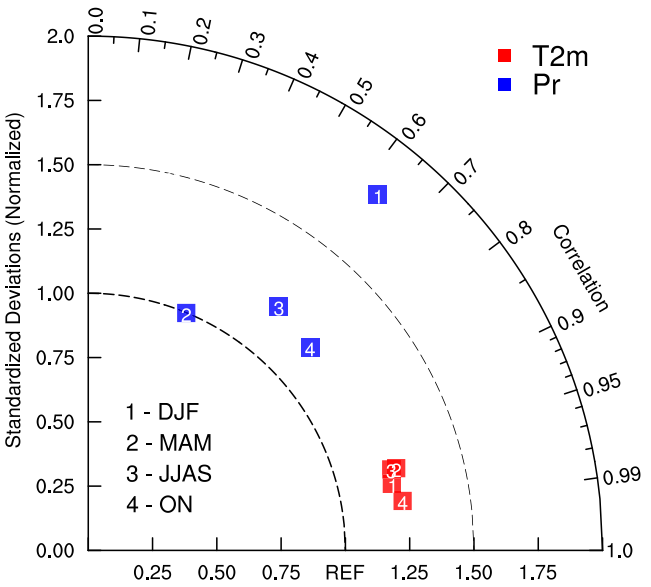

FIGURE 2 | Taylor diagram illustrating the 20-year climatology of four seasonal means (DJF: December–January–February, MAM: March–April–May, JJAS: June–July–August–September and ON: October–November) for precipitation (Pr; mm/day) and 2-m air temperature (T2m;°C) simulated by RSM-ROMS. The IMERG data and CRU TS v4.07 are used as the verification dataset for Pr and T2m, respectively. [Colour figure can be viewed at wileyonlinelibrary.com]

3.2 | Present-Day Simulations

In a recent study, Jayasankar, Misra, and Karmakar (2023) investigated the present-day JJAS mean climatology of precipitation, precipitable water vapour, 2-m air temperature (T2m), mean sea level pressure and zonal and meridional winds simulated by the RSM-ROMS. They found that the RSM-ROMS performs better than its parent GCM (CCSM4). We have used the Taylor diagram to compare the spatial pattern of mean climatology of simulated precipitation (Pr) and T2m across four seasons with IMD and 0.5° ×0.5° resolution CRU TS version 4.07 observations, respectively (Figure 2). The precipitation shows the highest pattern correlation coefficient (PCC) of 0.75 during ON and the lowest PCC during MAM (0.40). The simulated variances of Pr closely match observations for MAM, JJAS and ON, whereas for DJF, it slightly deviates from the observation. For the simulated T2m, the PCC exceeds 0.97 for all seasons, with ratios of standardised variance varying between 1.22 and 1.25 across the season.

In addition, we also evaluated the RSM-ROMS simulated Tmin (Figure 3a–d), Tmax (Figure 3e–h), T2m (Figure 3i–l) and Pr (Figure 3m–p) over Indian landmass against the corresponding IMD observations. The PCC of the 20-year climatology of the present-day climate (1986–2005) for Tmax (Tmin) between the RSM-ROMS and the corresponding IMD observation is 0.85 (0.83), 0.83 (0.84), 0.73 (0.77) and 0.84 (0.82), for DJF, MAM, JJAS and ON respectively. The spatial distribution of the climatology of seasonal mean Tmin shows that RSM-ROMS underestimate Tmin over most of the grid points across India during DJF (Figure 3a), MAM (Figure 3b) and ON (Figure 3d) seasons. But during the JJAS season (Figure 3c), RSM-ROMS tends to overestimate Tmin at most of the grid-points. Similarly, RSM-ROMS underestimated the mean Tmax at majority of the grid-points over India during DJF and ON seasons (Figure 3e,h). In contrast, during the MAM (Figure 3f) and JJAS seasons (Figure 3g), RSM-ROMS tends to overestimate Tmax at most of the grid points. The RSM-ROMS underestimate both the Tmin and Tmax over high-altitude regions in North and Northeast India where the IMD observation stations are also sparse. Similarly, T2m exhibits a negative bias during DJF and ON seasons (Figure 3i,l) across most grid-points. However, during the MAM and JJAS seasons (Figure 3j,k), many grid points show a positive bias, especially over the northern states of India. The systematic precipitation bias in the simulation shows a wet bias over Southeast Peninsular India during the DJF season (Figure 3m), which is when the region receives most of its rainfall. The RSM-ROMS shows a dry bias during the MAM season (Figure 3n) and a wet bias during the ON season (Figure 3p) across majority of the grid-points. During the JJAS season (Figure 3o), the model shows dry bias over Central India and wet bias over the western ghats and adjacent regions, which is a known issue with the atmospheric component of the RSM-ROMS (i.e., RSM, Jayasankar, Misra, and Karmakar 2023).

Figure 4 shows the simulated 20-year (1986–2005) climatological monthly mean Tmin and Tmax area averaged over the four regions. Overall, in most months, the model simulated Tmin and Tmax verify reasonably well with the observations. However, Tmin is consistently underestimated by the model in all four locations from January to May (Figure 4a–c). During April–June, the model overestimates Tmax in Region-1 (Figure 4e), Region-3 (Figure 4g) and Region-4 (Figure 4h). In contrast, in Region-2, the model clearly underestimates Tmax in January–March and September–December. In Region-4, the model underestimates Tmin throughout the year (Figure 4d), whereas Tmax is overestimated from mid-March to mid-June (Figure 4h). Also, unlike other regions, there exists a disparity between the IMD and CPC observations, which may be attributed to the lack of

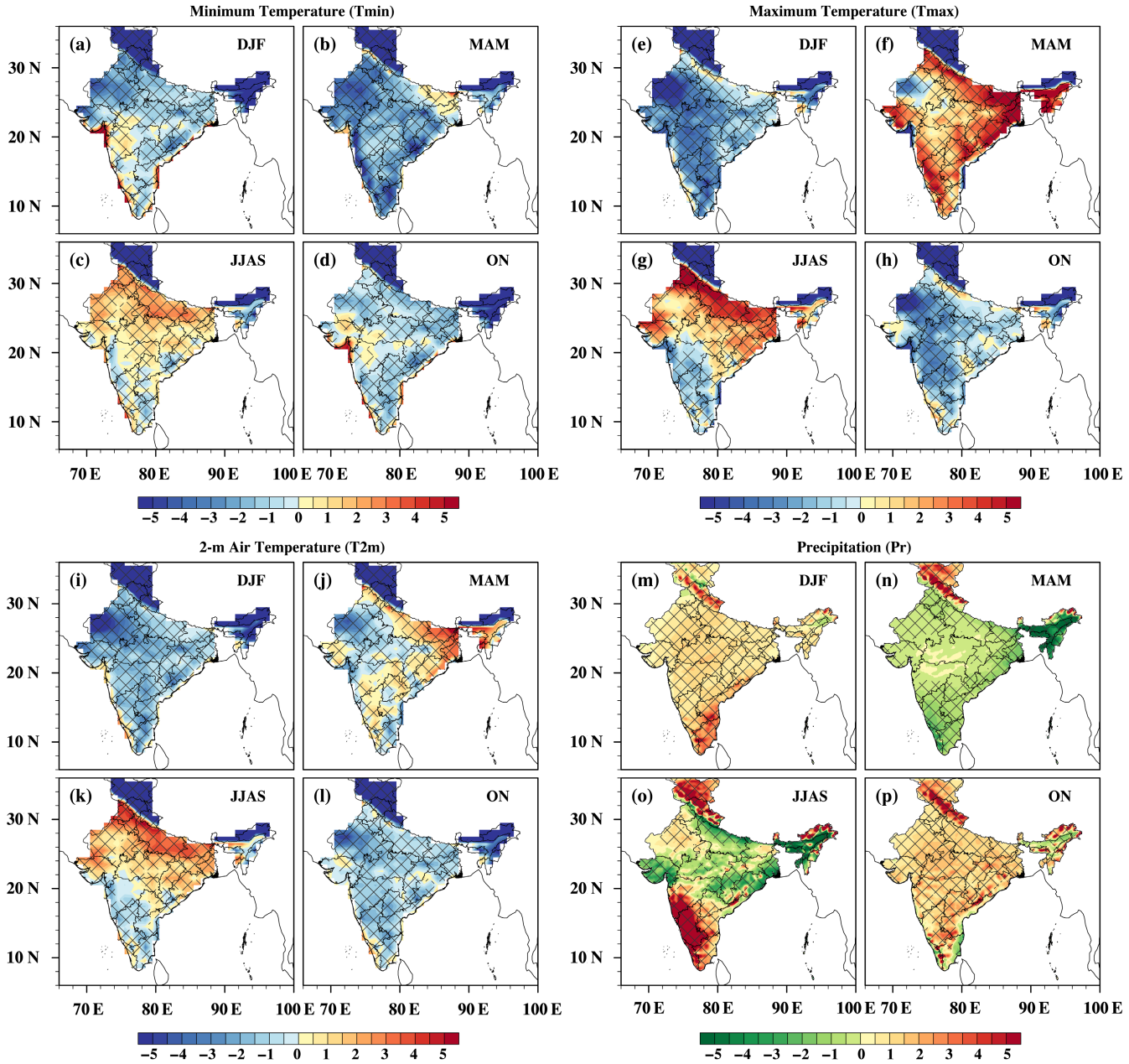

FIGURE 3 | Present-day 20-year climatological seasonal mean bias in (a–d) minimum temperature (°C), (e–h) maximum temperature (°C) and (i–l) 2-m air temperature (°C) with respect to IMD observations and (m–p) precipitation (mm/day) with respect to IMERG observation for (a, e, i, m) DJF, (b, f, j, n) MAM, (c, g, k, o) JJAS and (d, h, l, p) ON seasons. The hatched areas represent bias significant at a 5% significance level ($p = 0.05$) according to Student's *t*-test. [Colour figure can be viewed at wileyonlinelibrary.com]

sufficient in situ observations to constrain the varying analysis techniques.

3.3 | Projected Changes in DTR

Figure 5 exhibits the spatial distribution of the projected change (climatological difference between mid-21st century and historical simulations) in DTR. The statistical significance of the projected changes was determined using Student's *t*-test. During DJF season, the model projects a significant decrease in DTR over Region-1 (−0.86°C; Figure 5a) which is consistent with observed trends in the current climate. However, Region-2, Region-3 and Region-4 show a statistically insignificant change (Figure 5a). These patterns of change in DTR from RSM-ROMS can be understood from the corresponding change in Tmin and Tmax (Figure S3). For example, the projected decrease in DTR during DJF season in Region-1 is a result of significant warming in Tmin (Figure S3a–d) which is relatively smaller in Tmax (Figure S3e–h). Similarly, in the other regions, the change in DTR is relatively small because the projected change in Tmin and Tmax are comparable (Figure S3). In the MAM season, the majority of the grid points show insignificant projected changes in DTR (Figure 5). However, during the JJAS season, the model projects a significant decrease in DTR over Region-3 (−0.45°C; Figure 5c) aligning with observed trends, whereas the other three regions show insignificant changes. In the ON season, the majority of the grid points show a projected decrease

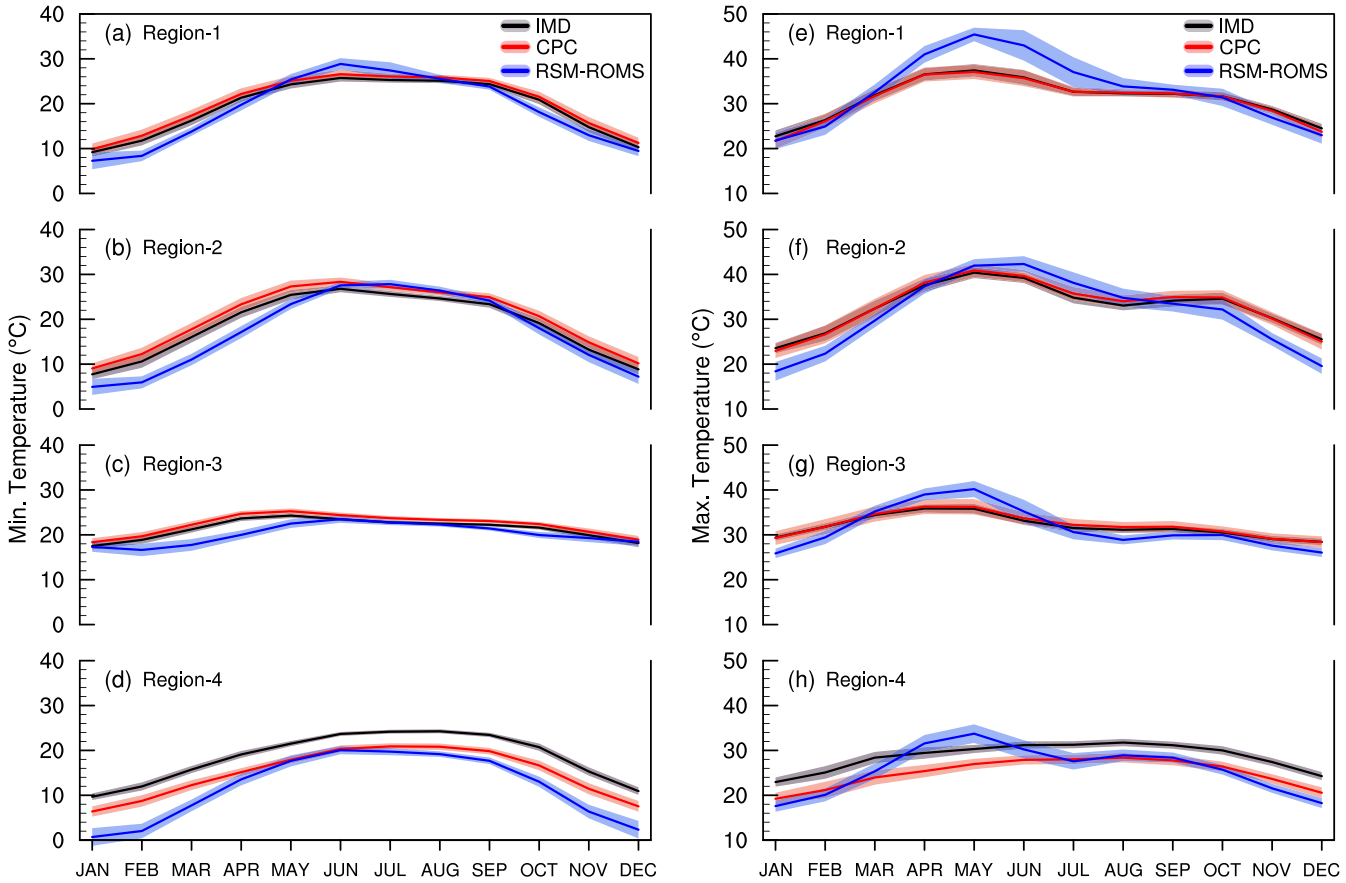

FIGURE 4 | Present-day 20-year (1986–2005) climatological monthly mean (a–d) minimum temperature (Tmin) and (e–g) maximum temperature (Tmax) area averaged over four regions. The solid lines in black, red and blue indicate the IMD observation, CPC observation and RSM-ROMS, respectively. Similarly, the standard deviations for IMD, CPC and RSM-ROMS are shaded as grey, red and blue, respectively. [Colour figure can be viewed at wileyonlinelibrary.com]

in DTR, particularly in peninsular India, northwest India, and parts of the Indo-Gangetic Plain. DTR decreases significantly in Region-1, Region-2 and Region-3 during ON, with reductions of −0.75°C, −0.77°C and −0.70°C, respectively. These projected decreases in DTR in ON is a result of the corresponding stronger warming in Tmin than in Tmax (Figure S3d,h). In contrast to the observed positive trend across all the seasons in Region-4 (Figure 1e–h), the model projects an insignificant future change in DTR over Region-4 (Figure 5). Again, these patterns of change in DTR across India from RSM-ROMS simulation can be easily understood from the projected near symmetrical changes in Tmin and Tmax (Figure S3). These results reaffirm the heterogeneous nature of the projected changes in DTR across India, which is in contrast with the findings of Lindvall and Svensson (2015). Lindvall and Svensson (2015) utilised the MME of CMIP5 models, which showed a significant reduction in annual DTR across India.

3.4 | Mechanism for Projected Changes

In this section, we attempt to understand the projected seasonal mean changes in DTR from a series of projected seasonal mean changes of related variables. For example, in Figure 6 we show the seasonal mean projected change in cloud cover (expressed as a % of grid coverage), area averaged over the four regions at the time of Tmin and Tmax, respectively. There are significant seasonal and regional variations in the projected cloud cover changes. For example, the total, middle and low cloud cover shows considerable seasonal variability across all four regions. In contrast, the high cloud cover shows a systematic increase over most regions and seasons (Figure 6d,h,l,p). Especially, in regions and seasons where the projected change in DTR is declining in Figure 5, we see that the high cloud cover is projected to increase both at the time of Tmax and Tmin, with a larger increase at the latter time. For example, in the ON season, Region-1, 2 and 3 or Region-1 in DJF or Region-3 in JJAS show an increase in the high cloud cover (Figure 6).

Because of the projected changes in the seasonal mean high cloud cover, there is an implication on the radiative fluxes (Figure 7). It may be noted that in computing these fluxes, the downward flux directed from atmosphere to surface is regarded as positive while the flux directed from surface to overlying atmosphere is regarded as negative. In terms of the corresponding seasonal mean radiative fluxes, the downward shortwave flux at the surface at the time of Tmax is projected to reduce over most regions and most seasons (Figure 7a,e,i,m). So, again focusing on regions and seasons when DTR declines in Figure 5, we see a projected decrease in downward shortwave flux in Region-1

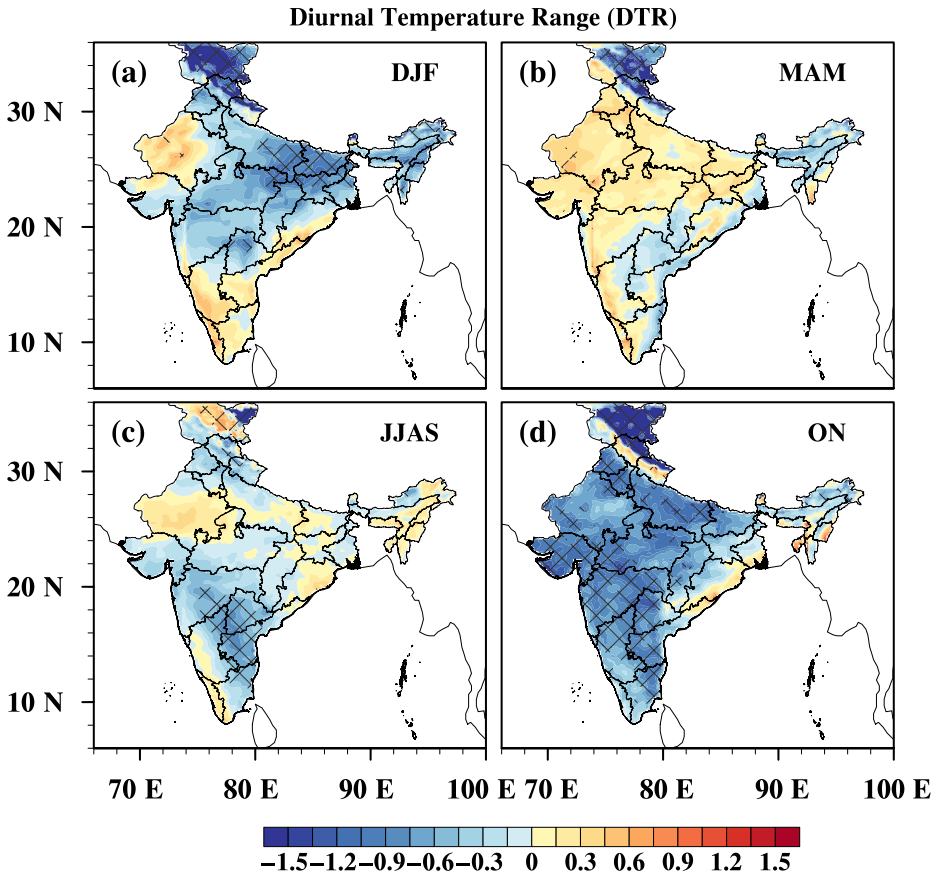

FIGURE 5 | Projected changes in DTR (°C) over the land at the mid-21st century (2041–2060) under RCP 8.5 scenario for (a) DJF, (b) MAM, (c) JJAS and (d) ON seasons. The hatched areas represent changes significant at a 5% significance level ($p = 0.05$) according to Student's *t*-test. [Colour figure can be viewed at wileyonlinelibrary.com]

in DJF, Region-3 in JJAS and across Region-1, Region-2 and Region-3 in ON. However, we also recognise the non-linear impacts of the projected changes in the water vapour content of the atmospheric column (not shown), mid and low-level cloud cover and their overlap with high clouds on the downward shortwave flux at the surface which are more difficult to attribute. However, the seasonal projected change in the upward shortwave flux at the time of Tmax nearly uniformly decreases over all regions across most seasons (Figure 7b,f,j,n). This suggests that there is likely a reduction in surface albedo in a future climate at the time of Tmax owing to an increase in soil moisture (discussed later in reference to Figure 9). It may be noted, however, that the changes in these shortwave flux terms are negligible at the time of Tmin.

On the other hand, the projected changes in the downward and upward longwave fluxes are comparable in Region-1 and Region-3 but much larger than the shortwave fluxes in the other two regions (Figure 7). Furthermore, they are of comparable magnitude at the time of Tmin and Tmax (Figure 7). The projected change in downward longwave flux at surface shows to uniformly increase across all regions and seasons at both times of Tmin and Tmax in the future climate. Similarly, the projected seasonal change in the upward longwave fluxes at the surface shows a uniform increase over all regions and seasons at both the time of Tmin and Tmax, which is also a reflection of increasing surface temperature in the future climate.

The corresponding projected changes in the enthalpy fluxes at the surface are shown in Figure 8. In focusing on regions and seasons where the DTR is projected to decline, we observe that the sensible heat flux decreases (Figure 8a–d) while latent heat flux increases (Figure 8e–h) at the time of Tmax. These enthalpy fluxes are much smaller at the time of Tmin. The corresponding projected change in top (10 cm) and root zone (1 m) soil moisture in Region-1 shows an increase at the time of Tmax (Figure 9). The wetter soil in the mid-21st century suggests a decrease in surface albedo that results in the reduction of the upward shortwave flux at surface, higher latent heat flux and lower sensible heat flux at the time of Tmax. It may be noted that in our simulations there is a projected increase in the Indian summer monsoon rainfall (Figure S4). In Region-2, the projected seasonal mean sensible heat flux increases while the latent heat flux reduces at the time of Tmax for most of the year (except in ON). This region is also marked by a reduction in the soil wetness (Figure 9). In Regions 3 and 4, the projected changes in sensible and latent heat flux show considerable seasonal variations, which is also marked by corresponding seasonal variations in the projected change in soil moisture.

In summary, the decline in projected DTR over Region-1 in DJF and ON and Region-3 in JJAS and ON is a result of asymmetrical projected increase in Tmin and Tmax, with larger increase in the former. These changes in Tmin and Tmax are associated

with increases in high cloud cover that reduce the downward shortwave flux, sensible heat and upward short wave fluxes while increase in the latent heat flux and downward longwave fluxes at the time of Tmax. Similarly, at the time of Tmin the downward long wave flux increases while there is a comparably weaker reduction in the upward longwave flux, which causes a stronger warming in Tmin than Tmax resulting in some of the regions in some seasons displaying a decrease in DTR over India.

3.5 | Diurnal Temperature Range Over Oceans

Figure 10a–d exhibits the spatial patterns of mean SST bias of RSM-ROMS from observation (OISST). The RSM-ROMS displays cooler SST over the northern Arabian Sea (AS; 0°–20° N and 58°–73° E) and Bay of Bengal (BoB; 0°—20° N and 86°—94° E) across all four seasons. However, the model exhibits a significant negative bias over the coasts of Oman and Pakistan during the DJF and MAM seasons. The mean bias over

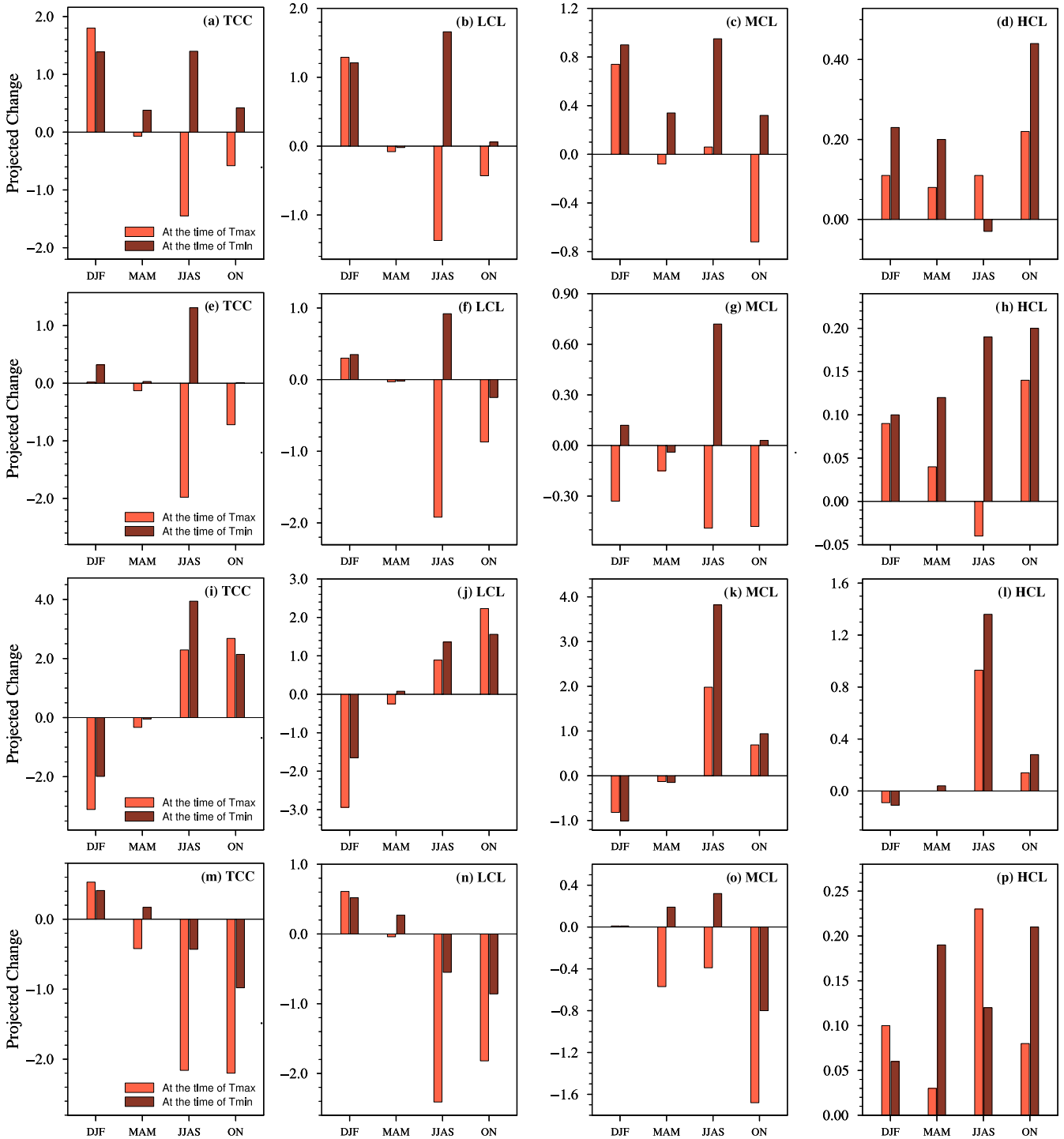

FIGURE 6 | Seasonal mean projected changes in total (TCC; a, e, i and m), low (LCL; b, f, j and n), mid-level (MCL; c, g, k and o) and high cloud cover (HCL; d, h, l and p) at the time of Tmax (pale red) Tmin (brown), which is area averaged for (a–d) Region-1, (e–h) Region-2, (i–l) Region-3 and (m–p) Region-4. The units are in % of grid coverage. [Colour figure can be viewed at wileyonlinelibrary.com]

AS and BoB is −0.08°C (−0.83°C) and −0.26°C (−0.37°C) for DJF (MAM) seasons. During DJF, the equatorial Indian Ocean is slightly warmer in the model. During the JJAS and ON seasons, the model shows warmer SST over the majority of AS and BoB than observed, with a significant positive bias (ranging between 0.5°C and 1°C) over the northern equatorial Indian Ocean. In contrast, the mean bias over AS and BoB is 0.24°C (0.25°C) and 0.50°C (0.38°C) for JJAS and ON seasons.

We analysed the model's simulated biases in Tmax (Figure 10e–h), Tmin (Figure 10i–l) and DTR (Figure 10m–p), over the ocean relative to the ERA5 reanalysis dataset. Similar to the SST bias, the model exhibits a significant negative Tmin bias along the coasts of Oman and Pakistan during the DJF and MAM seasons. The average Tmin bias across the AS and BoB is 0.23°C and 0.46°C for DJF (Figure 10e) and −1.16°C and −0.54°C for MAM (Figure 10f), respectively. In contrast, during

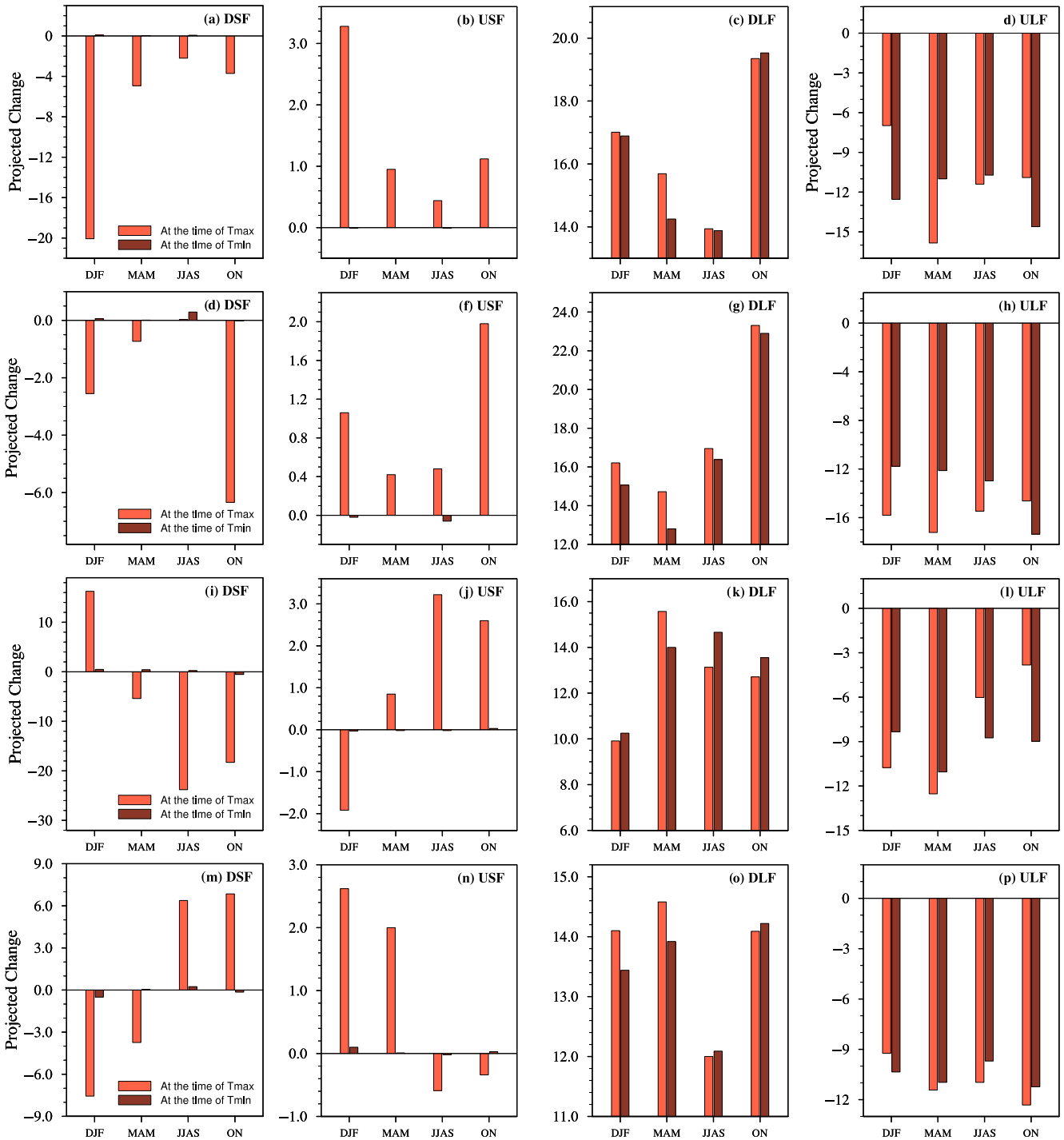

FIGURE 7 | Seasonal mean projected changes in downward shortwave (DSF; a, e, i and m), upward shortwave (USF; b, f, j and n), downward longwave (DLF; c, g, k and o) and upward longwave fluxes at the surface (ULF; d, h, l and p) at the time of Tmax (pale red) Tmin (brown), which is area averaged for (a–d) Region-1, (e–h) Region-2, (i–l) Region-3 and (m–p) Region-4. The units are in W/m^2. [Colour figure can be viewed at wileyonlinelibrary.com]

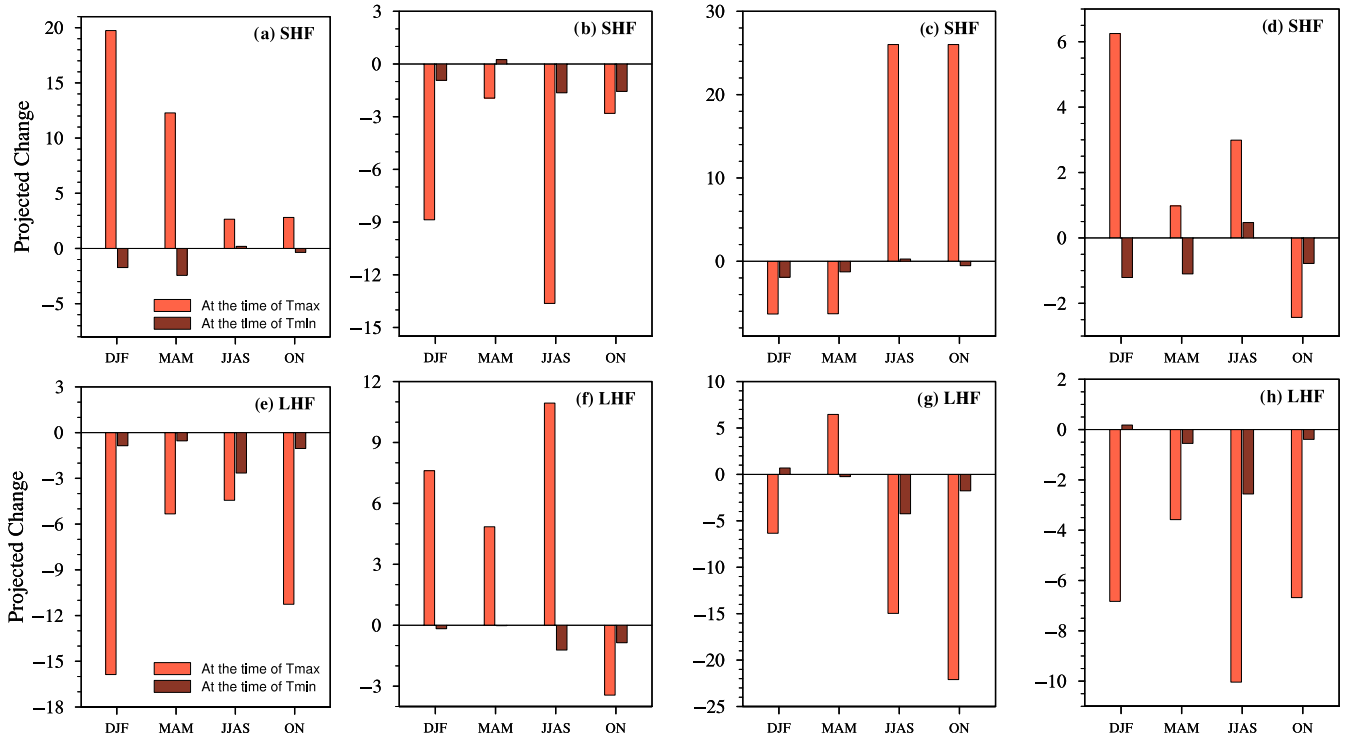

FIGURE 8 | Seasonal mean projected changes in sensible heat flux (SHF), and latent heat flux (LHF), at the time of Tmax (pale red) and Tmin (brown), which is area averaged for (a, e) Region-1, (b, f) Region-2, (c, g) Region-3 and (d, h) Region-4. The units are in W/m^2. [Colour figure can be viewed at wileyonlinelibrary.com]

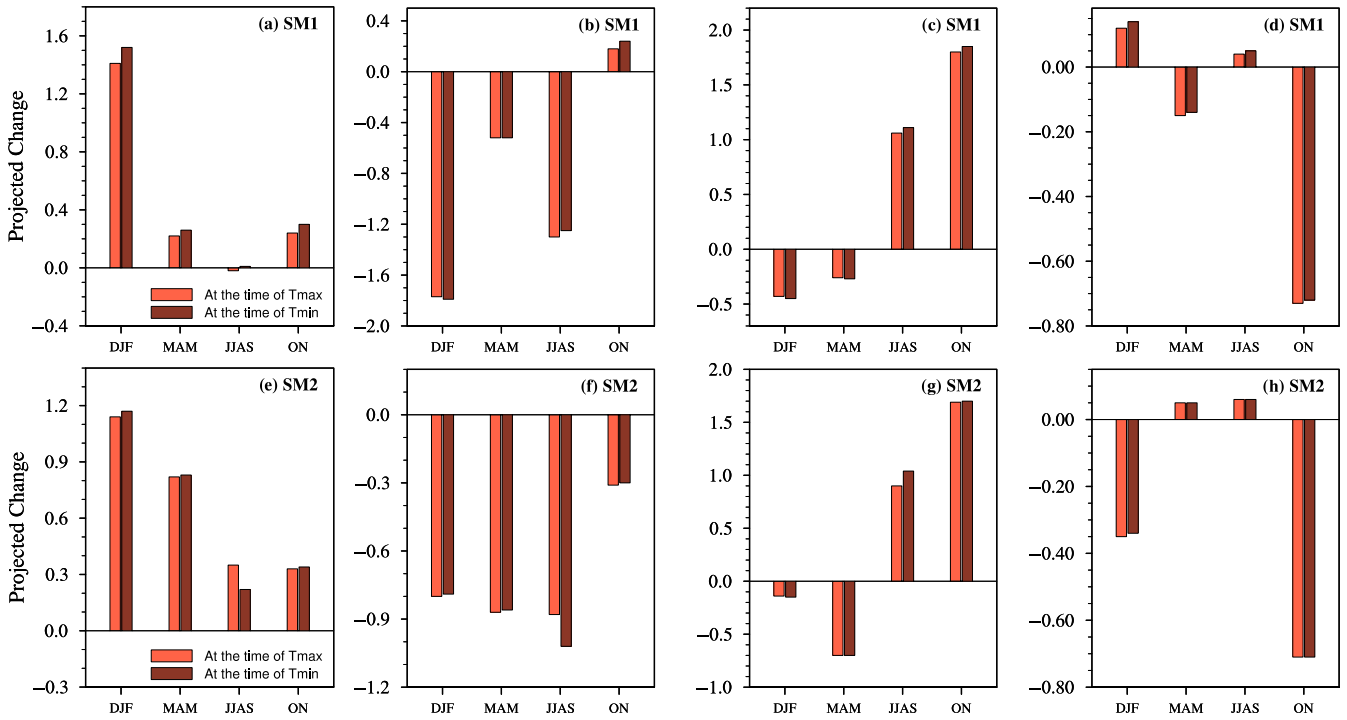

FIGURE 9 | Seasonal mean projected changes in the top (SM1; 10 cm) and root zone (SM2; 1 m) soil moisture at the time of Tmax (pale red) and Tmin (brown), which is area averaged for (a, e) Region-1, (b, f) Region-2, (c, g) Region-3 and (d, h) Region-4. The units are 100×fractions of grids. [Colour figure can be viewed at wileyonlinelibrary.com]

the JJAS and ON seasons, the model exhibits a positive Tmin bias over the majority of the Indian Ocean, with the BoB being warmer than the AS in both seasons (Figure 10g,h). The Tmin biases over AS are 0.33°C and 0.52°C during JJAS and ON and over BoB, it is 0.61°C and 1.01°C during JJAS and ON, respectively. The model shows a positive Tmax bias over the majority of the Indian Ocean during all four seasons, except for a few places having a negative bias around the coasts of Oman and

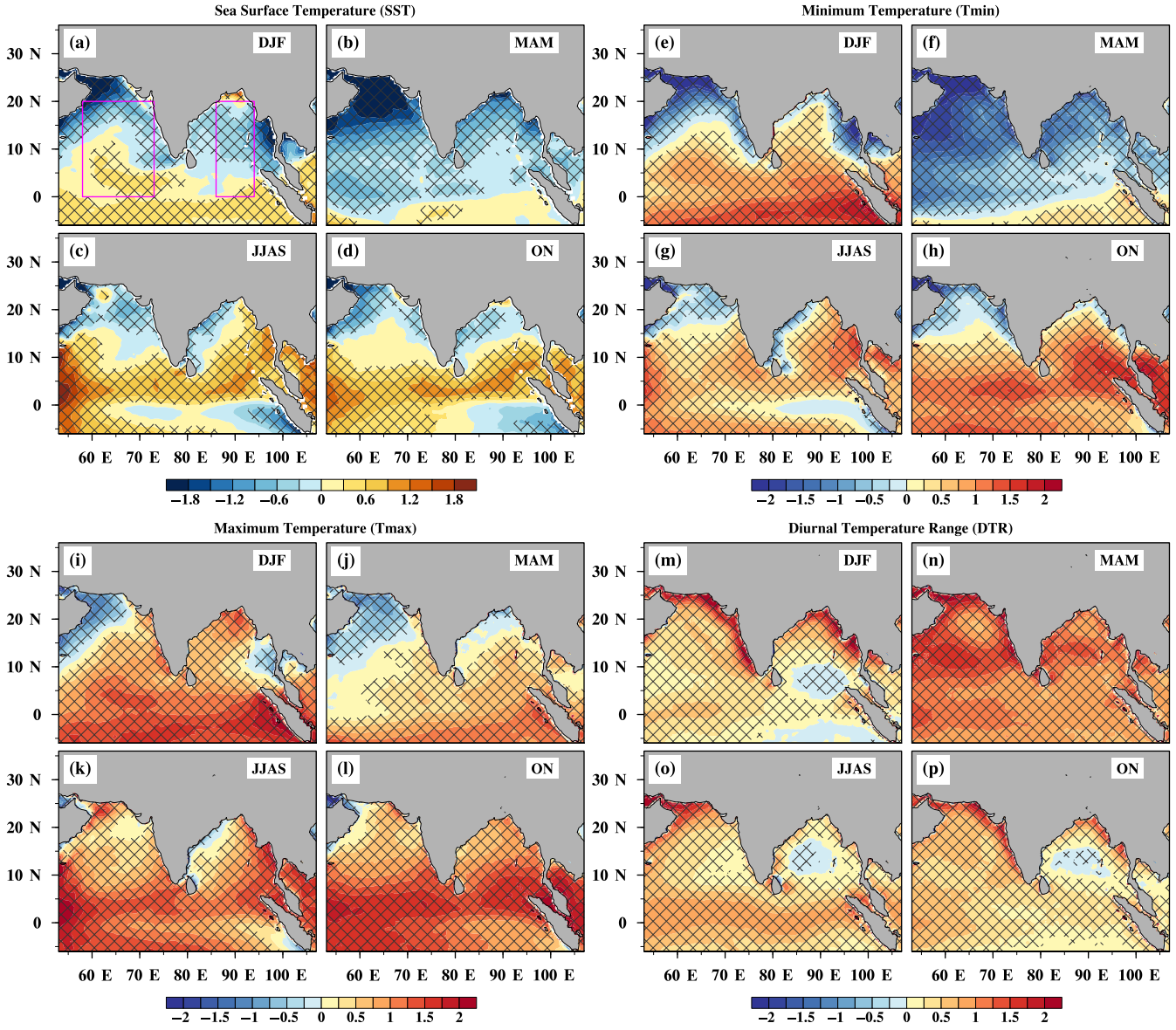

FIGURE 10 | Present-day 20-year climatological seasonal mean bias in (a–d) sea surface temperature (SST; °C) with respect to OISST, (e–h) minimum temperature (°C), (i–l) maximum temperature (°C) and (m–p) diurnal temperature range (DTR; °C) with respect to ERA5 reanalysis for (a, e, i, m) DJF, (b, f, j, n) MAM, (c, g, k, o) JJAS and (d, h, l, p) ON seasons. The areas considered for AS and BoB are shown (a) in magenta rectangular boxes. The hatched areas represent bias significant at a 5% significance level ($p = 0.05$) according to Student's *t*-test. [Colour figure can be viewed at wileyonlinelibrary.com]

Pakistan during the DJF and MAM seasons. The Tmax bias over the AS is 0.71°C, 0.06°C, 0.82°C and 1.07°C and over the BoB it is 0.77°C, 0.46°C, 0.88°C and 1.23°C for the DJF, MAM, JJAS and ON seasons, respectively. Similarly, the DTR bias is found to be slightly lower than the Tmin and Tmax bias. However, DTR bias is positive over the majority of the Indian Ocean during all four seasons. The DTR bias over the AS is 0.48°C, 1.23°C, 0.49°C and 0.56°C and over the BoB it is 0.31°C, 1.0°C, 0.27°C and 0.22°C for the DJF, MAM, JJAS and ON seasons, respectively. The highest DTR bias is found to be during the MAM season (Figure 10n).

Furthermore, in Figure 11, we looked at the projected changes in the DTR during the mid-21st century over the northern Indian Ocean under the RCP 8.5 scenario. The future DTR changes are found to be very small (and barely statistically significant) compared with land. For example, the projected changes in DTR over the AS is −0.01°C, 0.04°C, 0.02°C and 0.01°C and over the BoB it is −0.01°C, −0.01°C, −0.02°C and −0.03°C for the DJF, MAM, JJAS and ON seasons, respectively.

4 | Concluding Remarks

The analysis of the observed DTR climatology demonstrates that central and northwest India consistently display higher DTR (>15°C) during DJF, MAM and ON seasons, while Peninsular India and the eastern coast exhibit relatively lower values. On the other hand, the observed DTR during JJAS is low in comparison to the other seasons. Furthermore, we examined the observed trends in the DTR, which indicates

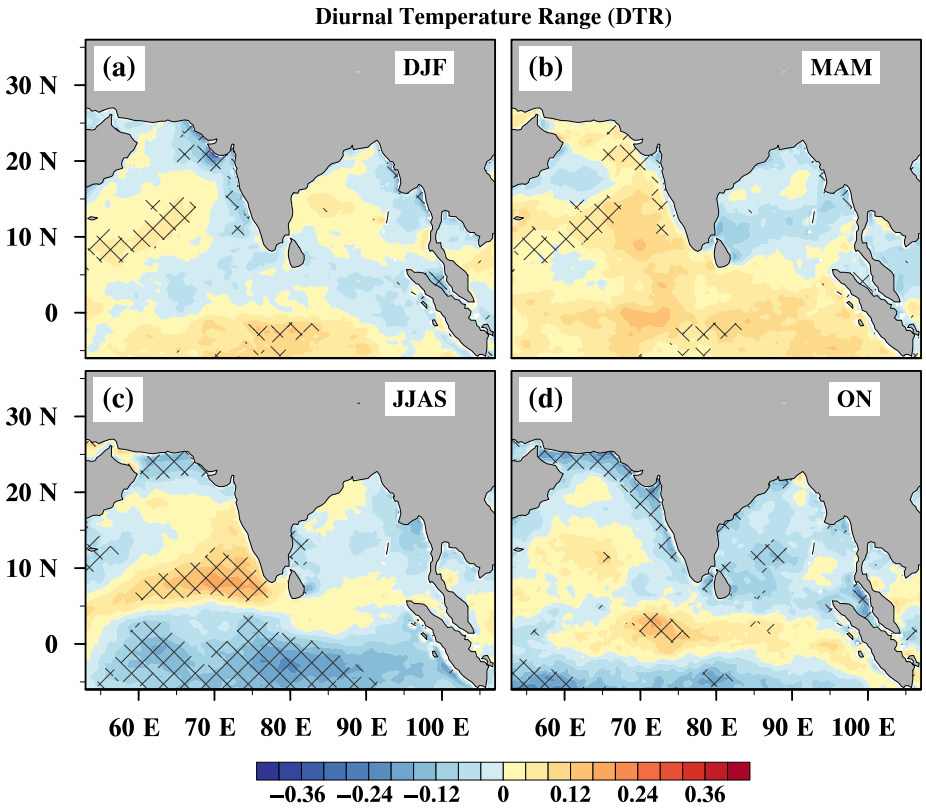

FIGURE 11 | Projected changes in DTR (°C) over the ocean at the mid-21st century (2041–2060) under RCP 8.5 scenario for (a) DJF, (b) MAM, (c) JJAS and (d) ON seasons. The hatched areas represent changes significant at a 5% significance level ($p = 0.05$) according to Student's t-test. [Colour figure can be viewed at wileyonlinelibrary.com]

a complex pattern throughout India's various regions and seasons, which is driven by asymmetrical trends in Tmin and Tmax. Region-1 and -2 exhibit a significant decreasing trend in DTR, particularly during the DJF and ON seasons, with the DJF season over Region-1 showing the highest decline (−0.52°C/decade). Many places in North, Northwest and Southern Peninsular India experience significant reductions in DTR during the DJF and ON seasons. In many of these regions, the warming trend of Tmin is far greater than the trend in Tmax. During the MAM season, however, Jammu and Kashmir, Northern Himachal Pradesh and Madhya Pradesh display a significant increase in DTR in the observations. Furthermore, during the JJAS season, Region-3 exhibits an observed decreasing trend of −0.08°C/decade. In contrast, Region-4 over northeast India exhibits a consistent increasing trend in DTR in the observations throughout the year. These results highlight the wide regional and seasonal differences in DTR trends across India.

This study utilises a coupled ocean–atmosphere RCM (i.e., RSM-ROMS), which has been extensively verified for its present-day climate simulation (Jayasankar, Misra, and Karmakar 2023) to assess the projected changes in DTR. The simulated seasonal mean climatology of precipitation and 2-m air temperature across four seasons from the RCM validate well with observed data. The 20-year mean climatology of mean Tmax and Tmin were evaluated against the observation, which revealed the PCC for Tmax is between 0.73 and 0.85, while the PCC for Tmin is between 0.77 and 0.84 for the different seasons of the year. The RCM shows reasonable skill in simulating the present-day Tmin and Tmax over the four regions considered in this study.

The RCM projects significant spatial variations in projected changes of DTR in the mid-21st century across different seasons and regions of India. DJF and ON seasons show significant decreases in DTR (from −0.73°C to −0.86°C) in certain regions (Regions 1, 2 and 3), whereas the MAM season shows insignificant changes across India. Region-3 exhibits significant decreases (−0.49°C) in DTR during JJAS, which is a continuation of the observed trends in the current climate. Region-4, however, shows a future reduction of DTR, especially during DJF, which contrasts with the observed increasing trend. The projected reduction in the DTR in all these regions across all seasons is mainly associated with asymmetrical projected warming of Tmax and Tmin.

In focusing over regions and seasons that displayed a significant projected decrease in DTR in the mid-21st century we find that the high cloud cover increases in such instances. In association with this increase, we find that the downward shortwave flux and upward shortwave flux is reduced, with the former being larger at the time of Tmax. Furthermore, at the time of Tmax, sensible heat flux reduces and latent heat flux increases in association with wet soil, from increased precipitation. These processes reduce the rate of warming of Tmax. Similarly, at time of Tmin, the downward longwave and upward longwave fluxes increase in the future climate, with the former dominating. The shortwave fluxes and enthalpy fluxes are comparatively weaker. Consequently, there is a surplus energy to increase the rate of warming of Tmin at these locations

and seasons, which results in DTR reducing in the future, mid-21st century climate. The model could simulate SST, Tmin, Tmax and DTR reasonably well over the northern Indian Ocean. The projected changes estimated for the mid-21st century over the AS and BoB were found to be relatively small and insignificant compared with the Indian landmass. Further research using several high-resolution regional climate models under different emission scenarios is recommended to better quantify potential uncertainties embedded in the projected changes in DTR and its spatial heterogeneity.

Author Contributions

C. B. Jayasankar: conceptualization, investigation, methodology, validation, software, formal analysis, data curation, visualization, writing – original draft, writing – review and editing. **Vasubandhu Misra:** conceptualization, supervision, resources, project administration, writing – review and editing, funding acquisition.

Acknowledgements

The present study was supported by NASA's Grants 80NSSC19K1199 and 80NSSC22K0595. We acknowledge the IMD for their minimum and maximum data, NOAA PSL, Boulder, Colorado, for the CPC minimum and maximum data and CRU (University of East Anglia) for the 2-m air temperature data, NASA GPM for the IMERG precipitation data. We thank three anonymous reviewers for their suggestions.

Conflicts of Interest

The authors declare no conflicts of interest.

Data Availability Statement

The India Meteorological Department (IMD) gridded (1×1) minimum and maximum temperature data set utilised for the analysis in this study is accessible from https://www.imdpune.gov.in/cmpg/Griddata/Min_1_Bin.html and https://www.imdpune.gov.in/cmpg/Griddata/Max_1_Bin.html. The daily minimum and maximum temperature from Climate Prediction Center (CPC) Global Unified Temperature Data is accessible from https://psl.noaa.gov. The monthly 2-m air temperature data is Climate Research Unit Timeseries (CRU TS) version 4.07 is accessible from https://crudata.uea.ac.uk/cru/data/hrg/cru_ts_4.07/. The daily IMERG precipitation data set used in this study is available at https://gpm.nasa.gov/data. The ERA5 reanalysis data at hourly intervals used in this study is available at https://doi.org/10.24381/cds.adbb2d47 (Hersbach et al. 2020). The OISST version 2 data used in this study is accessible from https://psl.noaa.gov/data/gridded/data.noaa.oisst.v2.highres.html (Huang et al. 2021). The RSM-ROMS simulation datasets for the analysis and to generate the figures shown in the paper are available from jcb@fsu.edu. All the final figures were created by utilising the NCAR Command Language v6.6.2 which is available via https://doi.org/10.5065/D6WD3XH5.

Endnotes

[1] We are forced in this instance to have a two-month season given that the summer monsoon is identified with 4 months.

References

Alpert, J., M. Kanamitsu, P. Caplan, J. Sela, and G. White. 1988. "Mountain Induced Gravity Wave Drag Parameterization in the NMC Medium Range Forecast Model." In *Conference on Numerical Weather Prediction*, 8th ed., 726–733. MD: Baltimore.

Bhutiyani, M. R., V. S. Kale, and N. J. Pawar. 2007. "Long-Term Trends in Maximum, Minimum and Mean Annual Air Temperatures Across the Northwestern Himalaya During the Twentieth Century." *Climatic Change* 85: 159–177.

Braganza, K., D. J. Karoly, and J. M. Arblaster. 2004. "Diurnal Temperature Range as an Index of Global Climate Change During the Twentieth Century." *Geophysical Research Letters* 31: L13217. https://doi.org/10.1029/2004GL019998.

Chou, M. D., and K. T. Lee. 1996. "Parameterizations for the Absorption of Solar Radiation by Water Vapor and Ozone." *Journal of the Atmospheric Sciences* 53, no. 8: 1203–1208.

Chou, M. D., and M. J. Suarez. 1994. "An Efficient Thermal Infrared Radiation Parameterization for Use in General Circulation Models." *NASA Technical Memorandum NASA-TM-104606* 3: 85.

Dai, A., K. E. Trenberth, and T. R. Karl. 1999. "Effects of Clouds, Soil Moisture, Precipitation, and Water Vapor on Diurnal Temperature Range." *Journal of Climate* 12, no. 8: 2451–2473.

Doan, Q.-V., F. Chen, Y. Asano, et al. 2022. "Causes for Asymmetric Warming of Sub-Diurnal Temperature Responding to Global Warming." *Geophysical Research Letters* 49: e2022GL100029.22.

Easterling, D. R., B. Horton, P. D. Jones, et al. 1997. "Maximum and Minimum Temperature Trends for the Globe." *Science* 277: 364–367.

Ek, M. B., K. E. Mitchell, Y. Lin, et al. 2003. "Implementation of Noah Land Surface Model Advances in the National Centers for Environmental Prediction Operational Mesoscale Eta Model." *Journal of Geophysical Research* 108, no. D22: 8851.

Ezer, T., H. Arango, and A. F. Shchepetkin. 2002. "Developments in Terrain-Following Ocean Models: Intercomparisons of Numerical Aspects." *Ocean Model* 4: 249–267.

Haidvogel, D. B., H. G. Arango, K. Hedstrom, A. Beckmann, P. Malanotte-Rizzoli, and A. F. Shchepetkin. 2000. "Model Evaluation Experiments in the North Atlantic Basin: Simulations in Nonlinear Terrain-Following Coordinates." *Dynamics of Atmospheres and Oceans* 32, no. 3: 239–281.

Hamal, K., S. Sharma, R. Talchabhadel, et al. 2021. "Trends in the Diurnal Temperature Range Over the Southern Slope of Central Himalaya: Retrospective and Prospective Evaluation." *Atmosphere* 12, no. 12: 1683.

Harris, I., T. J. Osborn, P. Jones, and D. Lister. 2020. "Version 4 of the CRU TS Monthly High-Resolution Gridded Multivariate Climate Dataset." *Scientific Data* 7: 109. https://doi.org/10.1038/s41597-020-0453-3.

Hersbach, H., B. Bell, P. Berrisford, et al. 2020. "The ERA5 Global Reanalysis." *Quarterly Journal of the Royal Meteorological Society* 146, no. 730: 1999–2049. https://doi.org/10.1002/qj.3803.

Hong, S. Y., and H. L. Pan. 1996. "Nonlocal Boundary Layer Vertical Diffusion in a Medium-Range Forecast Model." *Monthly Weather Review* 124, no. 10: 2322–2339.

Huang, B., C. Liu, V. Banzon, et al. 2021. "Improvements of the Daily Optimum Interpolation Sea Surface Temperature (DOISST) Version 2.1." *Journal of Climate* 34: 2923–2939. https://doi.org/10.1175/JCLI-D-20-0166.1.

Huang, X., R. J. Dunn, L. Z. Li, T. R. McVicar, C. Azorin-Molina, and Z. Zeng. 2023. "Increasing Global Terrestrial Diurnal Temperature Range for 1980–2021." *Geophysical Research Letters* 50, no. 11: e2023GL103503.

Huffman, G. J., R. F. Adler, D. T. Bolvin, et al. 2019. *Algorithm Theoretical Basis Document (ATBD) for Global Precipitation Climatology Project Version 3.0. Precipitation Data*. Greenbelt, MD: MEaSUREs project.

Jaswal, A. K., P. A. Kore, and V. Singh. 2016. "Trends in Diurnal Temperature Range Over India (1961–2010) and Their Relationship

With Low Cloud Cover and Rainy Days." *Journal of Climate Change* 2, no. 2: 35–55.

Jayasankar, C. B., V. Misra, and N. Karmakar. 2023. "A Comparative Study Between Regional Atmospheric Model Simulations Coupled and Uncoupled to a Regional Ocean Model of the Indian Summer Monsoon." *Earth and Space Science* 10, no. 4: e2022EA002733.

Jayasankar, C. B., K. Rajendran, and S. Surendran. 2018. "Monsoon Climate Change Projection for the Orographic West Coast of India Using High-Resolution Nested Dynamical Downscaling Model." *Journal of Geophysical Research: Atmospheres* 123, no. 15: 7821–7838.

Jhajharia, D., and V. P. Singh. 2011. "Trends in Temperature, Diurnal Temperature Range and Sunshine Duration in Northeast India." *International Journal of Climatology* 31, no. 9: 1353–1367.

Joy, A., and K. Satheesan. 2022. "Influence of Soil Moisture on Mean Daily Maximum and Minimum Temperatures Over India." *Meteorology and Atmospheric Physics* 134, no. 3: 49.

Juang, H. M. H., and M. Kanamitsu. 1994. "The NMC Nested Regional Spectral Model." *Monthly Weather Review* 122, no. 1: 3–26.

Karl, T. R., P. D. Jones, R. W. Knight, et al. 1993. "A New Perspective on Recent Global Warming: Asymmetric Trends of Daily Maximum and Minimum Temperature." *Bulletin of the American Meteorological Society* 74, no. 6: 1007–1024.

Lal, M., G. Srinivasan, and U. Cubasch. 1996. "Implications of Increasing Greenhouse Gases and Aerosols on the Diurnal Temperature Cycle of the Indian Subcontinent." *Current Science* 71, no. 10: 746–752.

Large, W. G., J. C. McWilliams, and S. C. Doney. 1994. "Oceanic Vertical Mixing: A Review and a Model With a Nonlocal Boundary Layer Parameterization." *Reviews of Geophysics* 32, no. 4: 363–403.

Li, H., and V. Misra. 2014. "Thirty-Two-Year Ocean–Atmosphere Coupled Downscaling of Global Reanalysis Over the Intra-American Seas." *Climate Dynamics* 43, no. 9–10: 2471–2489.

Lindvall, J., and G. Svensson. 2015. "The Diurnal Temperature Range in the CMIP5 Models." *Climate Dynamics* 44: 405–421.

Liu, J., X. Feng, X. Gu, J. Zhang, L. J. Slater, and D. Kong. 2022. "Detection and Attribution of Human Influence on the Global Diurnal Temperature Range Decline." *Geophysical Research Letters* 49, no. 13: e2021GL097155.

Lobell, D. B., C. Bonfils, and P. B. Duffy. 2007. "Climate Change Uncertainty for Daily Minimum and Maximum Temperatures: A Model Inter-Comparison." *Geophysical Research Letters* 34: L05715. https://doi.org/10.1029/2006GL028726.

Lobell, D. B., and J. I. Ortiz-Monasterio. 2007. "Impacts of Day Versus Night Temperatures on Spring Wheat Yields: A Comparison of Empirical and CERES Model Predictions in Three Locations." *Agronomy Journal* 99, no. 2: 469–477.

Mall, R. K., M. Chaturvedi, N. Singh, et al. 2021. "Evidence of Asymmetric Change in Diurnal Temperature Range in Recent Decades Over Different Agro-Climatic Zones of India." *International Journal of Climatology* 41, no. 4: 2597–2610.

Mellor, G. L., and T. Yamada. 1982. "Development of a Turbulence Closure Model for Geophysical Fluid Problems." *Reviews of Geophysics* 20: 851–875.

Misra, V., A. Mishra, and A. Bhardwaj. 2018. "Simulation of the Intraseasonal Variations of the Indian Summer Monsoon in a Regional Coupled Ocean–Atmosphere Model." *Journal of Climate* 31, no. 8: 3167–3185.

Moorthi, S., and M. J. Suarez. 1992. "Relaxed Arakawa-Schubert. A Parameterization of Moist Convection for General Circulation Models." *Monthly Weather Review* 120, no. 6: 978–1002.

Prakash, S., and H. Norouzi. 2020. "Land Surface Temperature Variability Across India: A Remote Sensing Satellite Perspective." *Theoretical and Applied Climatology* 139: 773–784.

Rai, A., M. K. Joshi, and A. C. Pandey. 2012. "Variations in Diurnal Temperature Range Over India: Under Global Warming Scenario." *Journal of Geophysical Research: Atmospheres* 117, no. D2: D02114.

Revadekar, J. V., D. R. Kothawale, S. K. Patwardhan, G. B. Pant, and K. Rupa Kumar. 2012. "About the Observed and Future Changes in Temperature Extremes Over India." *Natural Hazards* 60: 1133–1155.

Roy, S. S. 2019. "Spatial Patterns of Trends in Seasonal Extreme Temperatures in India During 1980–2010." *Weather and Climate Extremes* 24: 100203.

Roy, S. S., and R. C. Balling Jr. 2005. "Analysis of Trends in Maximum and Minimum Temperature, Diurnal Temperature Range, and Cloud Cover Over India." *Geophysical Research Letters* 32, no. 12: L12702.

Rupa Kumar, K., K. Krishna Kumar, and G. B. Pant. 1994. "Diurnal Asymmetry of Surface Temperature Trends Over India." *Geophysical Research Letters* 21: 677–680.

Shahfahad, B. A. A., M. W. Naikoo, S. Talukdar, J. Asif, Mallick, and A. Rahman. 2023. "Analysing Diurnal Temperature Range and Extreme Temperature Events Over Delhi and Mumbai Mega Cities." *Natural Hazards* 120: 1–29.

Shchepetkin, A. F., and J. C. McWilliams. 2005. "The Regional Oceanic Modeling System (ROMS): A Split-Explicit, Free-Surface, Topography-Following-Coordinate Oceanic Model." *Ocean Modelling* 9, no. 4: 347–404.

Sillmann, J., V. V. Kharin, X. Zhang, F. W. Zwiers, and D. Bronaugh. 2013. "Climate Extremes Indices in the CMIP5 Multimodel Ensemble: Part 1. Model Evaluation in the Present Climate." *Journal of Geophysical Research* 118: 1716–1733. https://doi.org/10.1002/jgrd.50203.

Singh, N., M. Chaturvedi, and R. K. Mall. 2023. "Unraveling Diurnal Asymmetry of Surface Temperature Under Warming Scenarios in Diverse Agroclimate Zones of India." *Theoretical and Applied Climatology* 152, no. 1–2: 321–335.

Solomon, S., D. Qin, M. Manning, et al., eds. 2007. "IPCC-AR4, IPCC: Climate Change 2007: The Scientific Basis." In *Contribution of Working Group I to the Fourth Assessment Report of the Intergovernmental Panel on Climate Change, Technical Report*. Cambridge: Cambridge University Press.

Srivastava, K., M. Rajeevan, and S. R. Kshirsagar. 2009. "Development of High-Resolution Daily Gridded Temperature Data Set (1969–2005) for the Indian Region." *Atmospheric Science Letters* 10: 249–254. https://doi.org/10.1002/asl.232.

Stone, D., and A. Weaver. 2003. "Factors Contributing to Diurnal Temperature Range Trends in Twentieth and Twenty-First Century Simulations of the CCCma Coupled Model." *Climate Dynamics* 20: 435–445.

Stone, D. A., and A. J. Weaver. 2002. "Daily Maximum and Minimum Temperature Trends in a Climate Model." *Geophysical Research Letters* 29: 1356. https://doi.org/10.1029/2001GL014556.

Tiedtke, M. 1983. "The Sensitivity of the Time-Mean Large-Scale Flow to Cumulus Convection in the ECMWF Model." In *Proceedings of ECMWF Workshop on Convective in Large-Scale Models*, 297–316. Reading, UK: European Centre for Medium-Range Weather Forecasts.

Umlauf, L., and H. Burchard. 2003. "A Generic Length-Scale Equation for Geophysical Turbulence Models." *Journal of Marine Research* 61, no. 2: 235–265.

Vinnarasi, R., C. T. Dhanya, A. Chakravorty, and A. AghaKouchak. 2017. "Unravelling Diurnal Asymmetry of Surface Temperature in Different Climate Zones." *Scientific Reports* 7: 7350.

Vose, R. S., D. R. Easterling, and B. Gleason. 2005. "Maximum and Minimum Temperature Trends for the Globe: An Update Through 2004." *Geophysical Research Letters* 32: L23822.

Wilkens, P., and U. Singh. 2001. "A Code-Level Analysis for Temperature Effects in the CERES Models." In *Modeling Temperature Response in Wheat and Maize*, edited by J. White, 1–7. El Batan, Mexico: CIMMYT.

Yang, J., H. Z. Liu, C. Q. Ou, et al. 2013. "Global Climate Change: Impact of Diurnal Temperature Range on Mortality in Guangzhou, China." *Environmental Pollution* 175: 131–136.

Zhao, Q., and F. H. Carr. 1997. "A Prognostic Cloud Scheme for Operational NWP Models." *Monthly Weather Review* 125, no. 8: 1931–1953.

Zhou, L., R. Dickinson, P. Dirmeyer, H. Chen, Y. Dai, and Y. Tian. 2008. "Asymmetric Response of Maximum and Minimum Temperatures to Soil Emissivity Change Over the Northern African Sahel in a GCM." *Geophysical Research Letters* 35, no. 5: L05402.

Supporting Information

Additional supporting information can be found online in the Supporting Information section.

Supporting Information for

Projected Changes in Diurnal Temperature Range Over India Using a Coupled Ocean-Atmosphere Regional Climate Model

C. B. Jayasankar[1,2] and Vasubandhu Misra[1,2,3]

[1]Center for Ocean-Atmospheric Prediction Studies, Florida State University, Tallahassee, FL, USA

[2]Florida Climate Institute, Florida State University, Tallahassee, FL, USA

[3]Department of Earth, Ocean and Atmospheric Science, Florida State University, Tallahassee, FL, USA

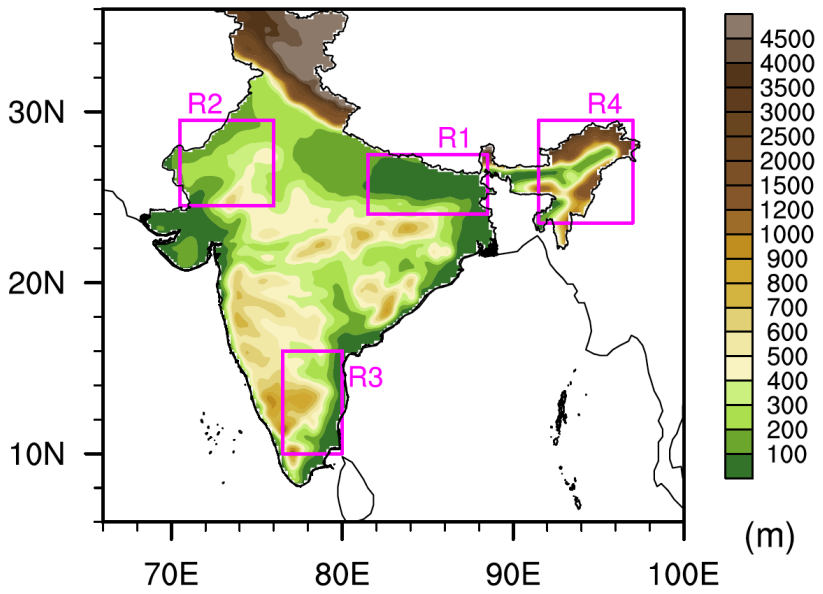

Figure S1. *The representation of topography (m) in RSM-ROMS is shown at 20 km grid spacing with four regions (Region–1 - R1, Region–2 - R2, Region–3 - R3, and Region–4 – R4) marked in Magenta color.*

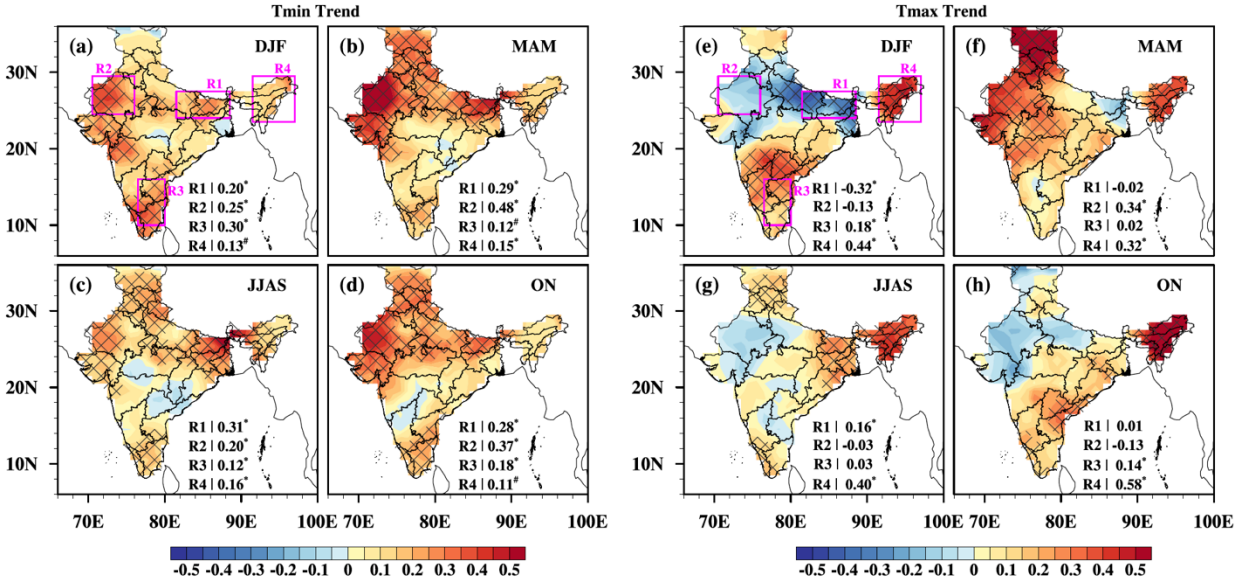

Figure S2: *Spatial distribution of 37-years (1986-2022) trend (°C/decade) in the Tmin (a-d) and Tmin (e-h) for a, e) DJF, b, f) MAM, c, g) JJAS, and d, h) ON seasons. The hatched areas represent trends significant at 5% significance level (p = 0.05) using the Mann-Kendall test.*

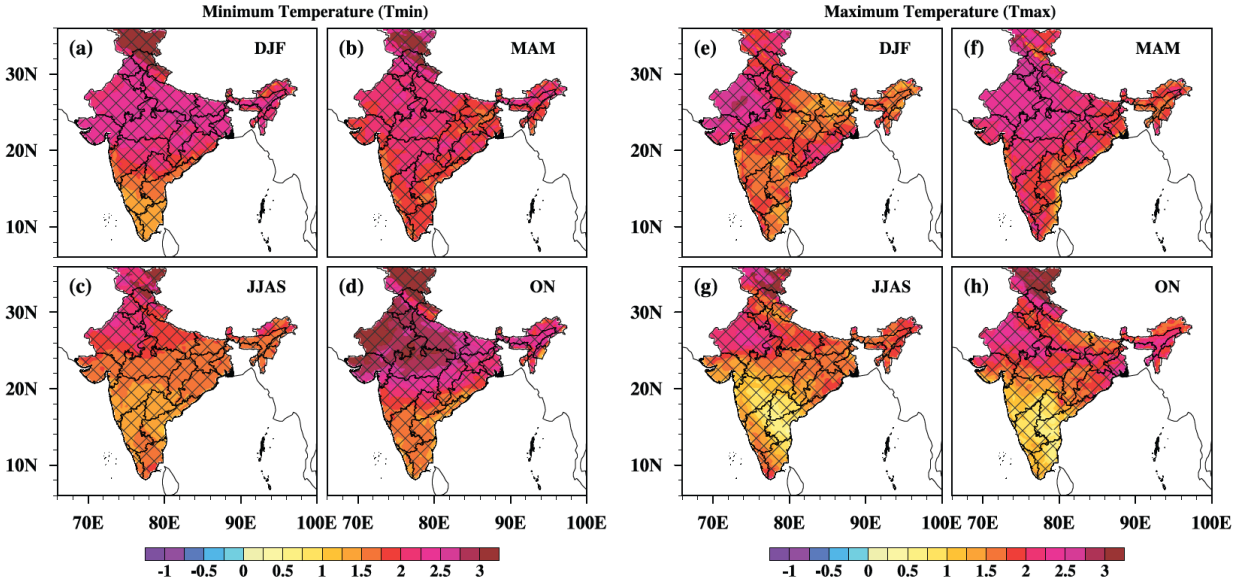

Figure S3. *Projected changes in Tmin (a-d) and Tmax (e-h) at the mid-21st century (2041-2060) under RCP8.5 scenario for a, e) DJF, b, f) MAM, c, g) JJAS, and d,h) ON seasons. The hatched areas represent changes significant at a 5% significance level (p = 0.05) according to Student's t-test.*

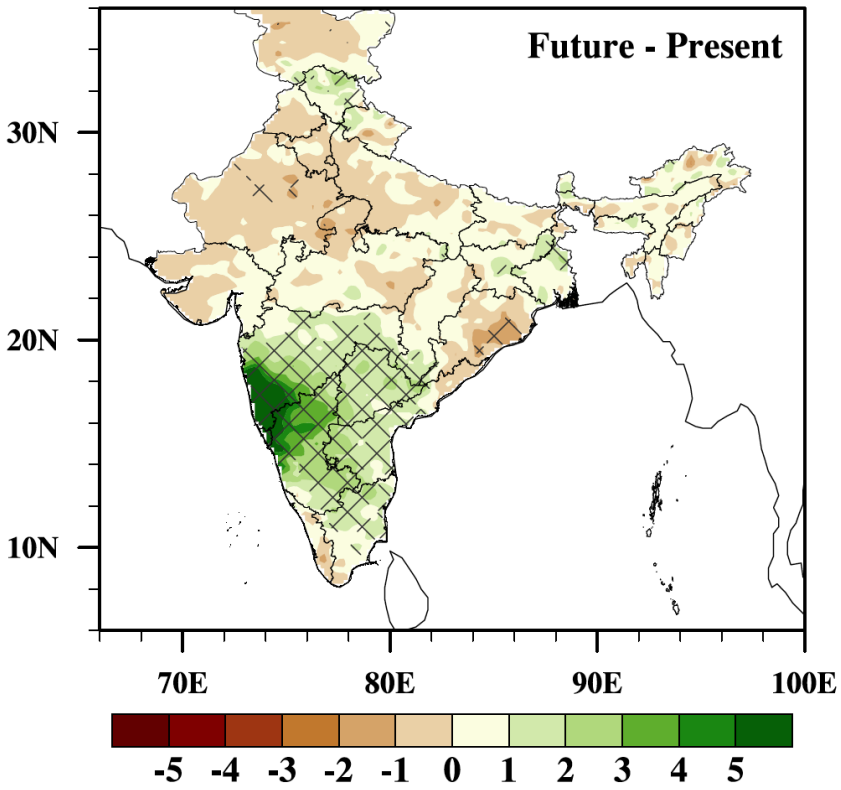

Figure S4: *The projected changes (future [2041-2060] minus present-day [1986-2005]) in Indian summer monsoon (June-September) rainfall (mm/day). The hatched areas represent changes significant at 5% significance level (p = 0.05) using the Student's t-test.*